EBioMedicine 56 (2020) 102783

Contents lists available at ScienceDirect

EBioMedicine

journal homepage: www.elsevier.com/locate/ebiom

Research paper

CD24-targeted intraoperative fluorescence image-guided surgery leads to improved cytoreduction of ovarian cancer in a preclinical orthotopic surgical model

Katrin Kleinmanns[a,1], Vibeke Fosse[a,b,1], Ben Davidson[c,d], Elvira García de Jalón[a,e], Olav Tenstad[f], Line Bjørge[a,g], Emmet McCormack[a,*]

[a] Center for Cancer Biomarkers, CCBIO, Department of Clinical Science, University of Bergen, Jonas Lies vei 91B, 5021 Bergen, Norway
[b] Department of Radiology, Erasmus Medical Centre, 3000 CA Rotterdam, the Netherlands
[c] Department of Pathology, Oslo University Hospital, Norwegian Radium Hospital, 0310 Oslo, Norway
[d] Faculty of Medicine, Institute of Clinical Medicine, University of Oslo, 0316 Oslo, Norway
[e] Department of Chemistry and Centre for Pharmacy, University of Bergen, Allégaten 41, 5007 Bergen, Norway
[f] Department of Biomedicine, University of Bergen, Jonas Lies vei 91B, 5021 Bergen, Norway
[g] Department of Obstetrics and Gyneacology, Haukeland University Hospital, 5021 Bergen, Norway

ARTICLE INFO

Article History:
Received 3 February 2020
Revised 3 April 2020
Accepted 21 April 2020
Available online 23 May 2020

Keywords:
Intraoperative imaging
Biomarker
Debulking surgery
Near-infrared fluorescence
HGSOC
Patient-derived xenograft

ABSTRACT

Background: The completeness of resection is a key prognostic indicator in patients with ovarian cancer, and the application of tumour-targeted fluorescence image-guided surgery (FIGS) has led to improved detection of peritoneal metastases during cytoreductive surgery. CD24 is highly expressed in ovarian cancer and has been shown to be a suitable biomarker for tumour-targeted imaging.
Methods: CD24 expression was investigated in cell lines and heterogenous patient-derived xenograft (PDX) tumour samples of high-grade serous ovarian carcinoma (HGSOC). After conjugation of the monoclonal antibody CD24 to the NIR dye Alexa Fluor 750 and the evaluation of the optimal pharmacological parameters (OV-90, n = 21), orthotopic HGSOC metastatic xenografts (OV-90, n = 16) underwent cytoreductive surgery with real-time feedback. The impact of intraoperative CD24-targeted fluorescence guidance was compared to white light and palpation alone, and the recurrence of disease was monitored post-operatively (OV-90, n = 12). CD24-AF750 was further evaluated in four clinically annotated orthotopic PDX models of metastatic HGSOC, to validate the translational potential for intraoperative guidance.
Findings: CD24-targeted intraoperative NIR FIGS significantly (47•3%) improved tumour detection and resection, and reduced the post-operative tumour burden compared to standard white-light surgery in orthotopic HGSOC xenografts. CD24-AF750 allowed identification of minuscule tumour lesions which were undetectable with the naked eye in four HGSOC PDX.
Interpretation: CD24-targeted FIGS has translational potential as an aid to improve debulking surgery of ovarian cancer.
Funding: This study was supported by the H2020 program MSCA-ITN [675743], Helse Vest RHF, and Helse Bergen HF [911809, 911852, 912171, 240222, 911974, HV1269], as well as by The Norwegian Cancer Society [182735], and The Research Council of Norway through its Centres of excellence funding scheme [223250, 262652].

1. Introduction

High-grade serous ovarian carcinoma (HGSOC) is the most common epithelial ovarian cancer (EOC) subtype and accounts for 80% of ovarian cancer deaths. Standard of care therapy typically consists of cytoreductive surgery followed by platinum-based chemotherapy. Recent progress in surgical efforts and the addition of anti-angiogenic agents and poly ADP-ribose polymerase (PARP) inhibitors as maintenance therapy for select patient groups have improved progression free survival [1]. However, despite these improvements the 5-year survival rate for HGSOC is still below 50%, with only modest increase of long-term survival rates over the last decades. Amongst the research priorities suggested for HGSOC to reduce mortality are enhanced definition of biomarkers which can predict surgical

* Corresponding author.
E-mail address: emmet.mc.cormack@uib.no (E. McCormack).
[1] These authors contributed equally to this work.

https://doi.org/10.1016/j.ebiom.2020.102783

Research in context

Evidence before this study

Ongoing clinical trials for folate-targeted fluorescence image-guided surgery (FIGS) in women with ovarian cancer are promising, and the improved detection of peritoneal lesions during cytoreductive surgery manifests hope of better outcome for these patients. Biomarkers which can distinguish malignancy from normal tissue with high specificity and sensitivity are a requirement for fluorescence assisted resections, and biomarkers of progenitor cells and metastasis are particularly relevant for debulking surgery of ovarian cancer. HER2, FSH, VEGF and osteonectin have all been evaluated as biomarkers for FIGS in preclinical EOC models. To further expand the palette of theranostic contrast agents available to surgeons in the intraoperative setting, we have investigated CD24, a stem cell marker, as a novel target for fluorescence-guided cytoreduction of ovarian cancer.

Added value of this study

We have demonstrated the benefit of CD24-targeted near-infrared FIGS in clinically relevant orthotopic xenograft and patient-derived xenograft models for high-grade serous ovarian carcinoma.

Implications of all the available evidence

We anticipate that the use of CD24-targeted FIGS will aid further delineation of metastases and be of greater benefit to ovarian cancer patients with poor prognosis. CD24 is overexpressed in many other solid tumours, highlighting the potential of CD24-FIGS as an aid during surgical resection of other cancers.

outcome, and optimisation of surgical debulkment [2]. Indeed, cytoreductive surgery represents the cornerstone of HGSOC therapy, with the volume of residual disease representing one of the most important prognostic factors for these patients [3]. Thus, the ultimate surgical goal in HGSOC is complete tumour resection, which unlike disease stage and molecular subtype, is the only clinical criteria influenced by the surgeon [4]. However, despite the efforts of the most skilled surgical practitioners, the impact of complete resection is also highly dependent on the patient's inherent tumour biology, immune status, and it is routinely hampered by disseminated carcinomatosis of the peritoneal cavity [5,6]. Consequently, the benefit and attributed complications of aggressive and radical upfront debulking surgery is currently being addressed by the TRUST international trial [7].

While significant efforts are currently being employed in the risk-stratification of patients that are most likely to benefit from immunotherapy [8] and those that will relapse following optimal surgery [3,7,9], improvement in surgical planning and imaging are also being developed [10]. Intraoperative imaging modalities for surgical guidance include ultrasound, x-ray fluoroscopic imaging, computed tomography (CT) or magnetic resonance imaging (MRI) [11]. However, these modalities are not tumour specific, and given the impracticality and cost of these techniques in the operative setting, surgeons still rely on subjective visual inspection and palpation of tissues intraoperatively to achieve complete resection. Thus, there is a critical need for more objective and practical technologies to increase the degree of cytoreduction for the vast majority of patients.

Fluorescence image-guided surgery (FIGS) is a relatively novel intraoperative molecular imaging modality to enter the surgical theatre [11,12]. FIGS exploits fluorescent contrast agents that label tumours either directly by binding to tumour biomarkers, or indirectly by accumulation due to enhanced permeability and retention (EPR) effect in solid tumours, resulting in dramatically enhanced visualisation of cancerous lesions, thus providing surgeons real-time guidance when performing complex oncologic resections [11,13,14]. Near-infrared (NIR) emitting fluorophores (700−900 nm) provide optimal contrast owing to low photon absorption, scattering, photobleaching and tissue autofluorescence, which maximises tissue penetration depth [15]. In addition, NIR fluorescence is invisible to the naked eye, and therefore does not impede the surgical field or operative procedures. van Dam et al. performed the first in-human clinical trial of FIGS targeting the folate receptor alpha (FRα) in patients with EOC [16,17]. Subsequently, a NIR conjugated probe of FRα (OTL38) has been examined in phase I and II clinical trials in EOC patients, demonstrating improved cytoreduction [18,19]. FIGS studies in preclinical EOC models have identified HER2, FSH, VEGF and osteonectin as alternative targets to folate [20−23], further expanding the palette of theranostic contrast agents amenable to surgeons in the intraoperative setting.

In the current study, we evaluate CD24, a small, heavily glycosylated, mucin-like cell surface protein which has been identified as a stem cell marker in ovarian cancer [24], as a target for NIR FIGS in orthotopic xenograft models of metastatic HGSOC. We have previously demonstrated the usefulness of non-invasive fluorescence imaging with CD24 conjugated to Alexa Fluor 680 [25], but due to autofluorescence in the 700 nm wavelength range during abdominal intraoperative imaging, we conjugated the human specific monoclonal antibody targeting CD24 to the longer wavelength NIR fluorophore Alexa Fluor 750 (CD24-AF750) in the current study. *In vitro* verification of CD24-AF750 targeting and subsequent *in vivo* pharmacokinetic and pharmacodynamic profiling of CD24-AF750 determined optimal contrast conditions for FIGS. We demonstrated the ability of CD24-AF750 to not only target primary tumours but also delineate local and distant metastases in relevant orthotopic xenograft models. Furthermore, we evaluated the impact of preclinical intraoperative FIGS with CD24-AF750 to improve surgical guidance and increase cytoreduction. Finally, we demonstrate the translational potential of CD24-AF750 to target heterogeneous patient-derived xenograft models of HGSOC.

2. Materials and methods

2.1. Conjugation of CD24-AF750 probe

The monoclonal mouse anti-human CD24 antibody (clone SN3, cat# MCA1379ELX, RRID: AB_321526, Bio-Rad, Oxfordshire, UK) was conjugated to Alexa Fluor® 750 NHS ester using the SAIVI™ rapid antibody labelling kit and purified by size exclusion chromatography as described by the manufacturer (cat# S30046, Invitrogen, Carlsbad, USA). The spectral characteristics of the resulting protein, CD24-AF750, was determined (Supplementary Fig S1a; λ_{ab} = 753 ± 3 nm, λ_{em} = 778 ± 2 nm) by Spark 20 M (Tecan, Männendorf, Switerland) and the final conjugate concentration (1•6 μg/μl), the degree of labelling (DOL = 3•26 ± 0•04) and the protein recovery (68 ± 7•35%) was measured and calculated photometrically by the One UV−Vis spectrophotometer (λ_{280} protein/λ_{753} dye, Thermo Scientific™, Waltham, USA). The conjugation efficiency and the purity of the conjugate were further validated by high performance liquid chromatography (HPLC). High resolution size exclusion chromatography was performed using a 4•6 mm ID × 30•0 cm L TSK gel Super SW3000 column and a 4•6 mm ID × 3•5 cm L Guard (part numbers 18675 and 18762, Tosoh Bioscience, Griesheim, Germany) with an optimal separation range for globular proteins of 10−500 kDa. The analysis was carried out using 0•1 mol/L Na_2SO_4 in 0•1 mol/L Phosphate buffer at pH 6•7 as mobile phase with a flow rate of 0•35 mL/min (Thermo Scientific™ Dionex™ UltiMate™ LPG-3400SD Pump). A Thermo Scientific™ Dionex™ UltiMate™ 3000 Rapid Separation

Diode Array Detector in the wavelength range 200−800 nm was used and the data were collected and processed employing the Chromeleon™ Chromatography Data System (CDS) Software (version 7.2.10). Based on the elution volumes and times (not shown) obtained for the different analytes (CD24, AF750 and CD24-AF750) no traces of free dye were present in the conjugate sample (Supplementary Fig. S1b).

2.2. Cell lines and cell culture

Human EOC cell lines Caov-3 (cat# HTB-75, RRID: CVCL_0201), OV-90 (cat# CRL-11732, RRID: CVCL_3768), and Skov-3 (cat# HTB-77, RRID: CVCL_0532) were obtained from the American Type Culture Collection (ATCC Manassas, VA, USA), and COV318 (cat# 07071903, RRID: CVCL_2419) from Sigma Aldrich (Sigma Aldrich, St. Louis, USA). The cell lines were cultured in RPMI 1640 (OV-90) and DMEM (Caov-3, Skov-3 and COV318) media supplemented with 10% heat-inactivated FBS and 1% L-glutamine for at least one week (3−7 passages) before included into *in vitro* or *in vivo* studies (RPMI cat# R5886, DMEM cat# D5671, Sigma Aldrich) (FBS cat# 10270106, L-Glutamine cat# 25030081, Gibco, Paisley, UK). Mycoplasma testing was performed using the MycoAlert™ PLUS assay (cat# LT07-705, Lonza, Walkersville, USA). All cell lines were transduced to express green fluorescent protein (GFP) and red-shifted *Luciola Italica* luciferase; performed according to the manufacturers protocol using the Redi-Fect Red-FLuc-GFP lentiviral particles (cat# CLS960003, Perkin Elmer, Waltham, MA, USA). Stable expression of luciferase allowed for non-invasive *in vivo* monitoring of tumour growth by bioluminescence imaging.

2.3. Patient material

Patient-derived xenograft (PDX) models of HGSOC were developed from tumour tissue obtained from chemotherapy naïve patients with primary advanced disease, admitted to the Department of Obstetrics and Gynaecology, Haukeland University, Bergen, Norway. The tumour specimens were included in the Bergen Gynaecologic Cancer Biobank. Informed consent was obtained from the women before collection of the fresh tumour samples. The regional committees for medical and health research ethics (REC West) has approved the biobank and the study (Reference IDs: 2014/1907, 2015/548 and 2017/612). Resected tumour samples were processed immediately. Tumour samples were cut into small pieces (2 mm^3) using a sterile scalpel and washed with phosphate buffered saline (PBS). Tissue pieces were enzymatically dissociated for two hours with collagenase II (cat# 17101015, 300 U/mL, Gibco) supplemented with 3 mM activity stabiliser $CaCl_2$, followed by addition of TrypLE (cat# 12604013, Gibco) on continuous agitation for 10 min (250 rpm, 37 °C). Dissociated cells were strained, washed with PBS, checked for cell viability with trypan blue staining, and stored in freezing medium (90% FBS, 10% DMSO) at −150 °C.

2.4. Flow cytometry analysis

EOC cell suspensions (OV-90, Caov-3, COV318 and Skov-3) were detached from culture flasks with 1× trypsin (cat# T3924, Sigma Aldrich), washed, and re-suspended in FACS staining buffer (PBS supplemented with 5% FBS and 2 mM EDTA). Before staining, 2×10^5 cells were incubated with 10% human FcR blocking reagent (cat # 130-059-901, Miltenyi Biotec, Bergisch Gladbach, Germany) for 5 min and stained with CD24-AF750 (1 μg) in a staining volume of 100 μL for 20 min at 4 °C. Mouse anti-human CD24-PE (clone SN3, 7•5 μL/0•37 μg, cat # LS-C105830, RRID: AB_1053866, LS Bio, Seattle, USA) was used as a positive control. All samples were washed twice with FACS staining buffer and acquired with the BD Fortessa Flow cytometer (BD Biosciences, Franklin Lakes, NJ, USA).

Quantitative determination of CD24 expression of OV-90 cells, expressed as antibody-binding capacity (ABC) units, was performed by using a bead calibration kit (Qifikit cat# K007811-8, Dako Agilent, Santa Clara, USA). 10^5 cells were re-suspended in 100 μL FACS buffer and stained with a saturated concentration of 5 μg unconjugated mouse anti-human CD24 for 45 min at 4 °C. An unconjugated monoclonal CD33 IgG1 antibody (Clone WM53, Cat# MCA1271T, RRID: AB_2074234, Bio-Rad) was used as a negative control. Cells, set-up beads and calibration beads were washed with PBS-BSA-Azide buffer twice and stained with a secondary FITC conjugate (provided in the Qifikit) for 45 min at 4 °C. After two further washing steps, samples were acquired and recorded with the BD Fortessa Flow cytometer.

2.5. In vitro *targeting of CD24*

The binding affinity of CD24-AF750 to EOC cell lines (OV-90, Caov-3, COV318 and Skov-3) was determined by optical fluorescent imaging (FLI), and comparison of CD24-AF750 to CD24-IRDye 800CW was performed after conjugation of the mAb CD24 to IRDye® 800CW NHS ester (cat# 929-70020, lot# C90927-04, LI-COR, Lincoln, NE, USA) with a DOL of 3•3. Briefly, cells were detached, washed and $2•5 \times 10^6$ cells were stained with 1μg of either CD24-AF750 (as previously described), or CD24-IRDye 800CW. Cells were washed twice and kept in cell pellets without supernatant before being imaged with the IVIS Spectrum *In Vivo* Imaging System, PerkinElmer, using the filter settings λ_{ex} = 745 ± 15 nm, λ_{em} = 800 ± 10 nm, and NIR channel #2 in the FLARE® intraoperative near-infrared fluorescence imaging system RP1 (Fluorescence-Assisted Resection and Exploration imaging system, Curadel LLC, Marlborough, USA), which has a laser excitation source λ_{ex} = 760 ± 3 nm and an imaging filter ≥ 781 nm (Supplementary Fig. S1a).

2.6. In vitro *cell proliferation assay at different CD24-AF750 concentrations*

In vitro OV-90 cell proliferation was evaluated in the presence of 10^{-10}– 10^{-7} M CD24-AF750 to test the safety of the conjugate. A water soluble tetrazolium salts (WST-1) assay (cat # 5015944001, Roche Applied Science, Pensberg, Germany) was used to validate cell proliferation 48 h after the incubation with four different CD24-AF750 concentrations (4 h after WST-1 incubation) and performed according to the manufacturers protocol and as previously described [25]. The spectrophotometrically measured formazan signal concentration of all metabolically active cells of all samples were normalised to 48-h cultures of OV-90 cells without CD24-AF750.

2.7. In vivo *xenograft models of ovarian cancer*

All animal experiments were conducted in compliance with the procedures of the Norwegian State Commission for Laboratory Animals, the European Convention for the Protection of Vertebrates Used for Scientific Purposes and approved by the Norwegian Food Safety Authority (Application ID 14128). Female NOD-*scid* IL2rγ^{null} (NSG) mice (aged 8 to 12-weeks, weight 22•59 ± 2•08 g; Vivarium, University of Bergen) were maintained under defined floral conditions and housed in individually ventilated (HEPA-filtered air) cages at the University of Bergen's animal facility. No more than five mice were in each individually ventilated cage, which was kept on a 12-h dark/night schedule at a constant temperature of 21 °C and at 50% relative humidity. Bedding and cages were autoclaved and changed twice per month, and the mice had continuous supply of sterile water and food. The animals were monitored daily by the same personnel for the duration of the experiment and weighed twice weekly. Activity levels, appearance, food intake and post-operative wounds were monitored, and humane endpoints were defined with the use of

score sheets. When indicated, animals were euthanised according to institutional guidelines.

2.7.1. Subcutaneous xenograft model

The NSG mice were injected with 5×10^6 OV-90^{luc+} cells re-suspended in 150 μL 1:1 saline/matrigel mix (cat# 08-774-391, Corning Inc®, Fisher Scientific, Waltham, USA) subcutaneously in the left flank under 3•5% sevoflurane anaesthesia (cat# 29960 SevoFlo, Zoetis, Louvain-la-Neuve, Belgium). Mice were included in FLI experiments when the calliper measurements reached 200 mm^3 (Volume = (height × width × length × π)/6).

2.7.2. Orthotopic xenograft model

Mice were anaesthetised as described above and placed in left lateral recumbence. A combination protocol for analgesia, including 0•1 mg/kg buprenorphine hydrochloride (cat# 561634 Temgesic, Indivor UK Ltd, Slough, Berks, Great Britain) and 5 mg/kg meloxicam (cat# 386860 Metacam vet., Boehringer Ingelheim Animal Health Nordics, Copenhagen, Denmark) was administered subcutaneously. The fur on the right flank was shaved and the skin was prepared aseptically with chlorhexidine 5 mg/mL (cat# 007169 Fresenius Kabi, Halden, Norway). The surgical procedure was performed as previously described [26], with the following modifications; 10^5 OV-90^{luc+} cells or single cell suspensions from four different primary tumours were separately mixed with matrigel (1:1, cat# 08-774-391, Corning Inc®, Fisher Scientific, Waltham, USA) and injected into the bursa of the ovary at the level of the oviduct, using a 30 G needle. Abdominal muscles and skin were closed separately, using 6–0 absorbable polyglactin suture (cat# V492H Vicryl, Ethicon, Johnson & Johnson, Belgium). The animals were given a subcutaneous injection of sterile saline and allowed to recover in a warm environment, before returning to the home cage.

2.8. In vivo *imaging*

2.8.1. Bioluminescence imaging

Bioluminescence imaging (BLI) was performed using the IVIS Spectrum *In Vivo* Imaging System, 10 min after intraperitoneal administration of 150 mg/kg of D-luciferin (cat# L-8220, Biosynth, Staad, Switzerland). Tumour progression for animals xenografted with luciferase positive OV-90^{luc+} cell lines was monitored weekly following injection, and after debulking surgery.

2.8.2. Fluorescence imaging

CD24-AF750 at a concentration of 3 μg/g mouse bodyweight was injected intravenously into the tail vein. FLI was performed with the IVIS Spectrum *In Vivo* Imaging System with a 745 ± 15 nm excitation bandpass filter and 800 ± 10 nm emission bandpass filter, 48 h after monoclonal antibody administration, or as indicated. All scans were acquired with epi-illumination and auto exposure. For bioluminescence and fluorescence optical imaging data, region of interests (ROI) were manually gated around the tumour, the organ, the background (muscle) or the whole ventral and lateral positioned mouse and calculated using the Living image software (Perkin Elmer). The mean fluorescence intensity and tumour to background ratio was calculated at different time points.

2.8.3. Intraoperative NIR fluorescence imaging

Intraoperative imaging was performed using the FLARE® intraoperative NIR fluorescence imaging system (Curadel LLC). Acquisition of CD24-AF750 fluorescence was conducted using NIR channel #2, as described above; exposure time was set to 500 ms and gain to 1. The colour video channel has a 400–660 nm illumination source; exposure time was set to 8.5 ms. Both images were simultaneously acquired and merged as a pseudo-coloured image. The imaging head was positioned at 24•5 cm working distance, resulting in a field of view (FOV) of 7•7 cm^2 (no zoom). Intraoperative images were analysed using ImageJ (Fiji, version 1.52p,) and the FLARE internal analysis software (V3.5.0). The fluorescence intensity was measured in arbitrary units (A.U.) and illustrated as mean fluorescence intensity. Tumour to background ratios (TBR), liver to background ratios (LBR) and tumour to liver ratios (TLR) were measured using the FLARE software, the background was defined as the signal intensity of the adjacent tissue or muscle.

2.8.4. Determination of NIR optimal contrast

For the *in vivo* CD24-AF750 biodistribution (n = 9), dose finding study (n = 12, 1 μg, 2 μg, 3 μg and 4 μg antibody per gram mouse bodyweight) and patient-derived xenograft models (n = 10), mice were injected intravenously with CD24-AF750 48 h prior to imaging, or as otherwise indicated. Anaesthesia was provided as described for the surgical protocols. A midline coelitomy was performed, and intraoperative CD24-AF750 fluorescence imaging was performed as described above. Mice were euthanised, and tumours and abdominal organs were imaged *ex vivo* with the FLARE system and IVIS for confirmation of fluorescence specificity. Resected tumour tissue was inoculated in D-luciferin for 10 min and BLI (IVIS) was performed for confirmation of OV-90^{luc+} origin.

2.8.5. Intraoperative FIGS – survival study

Orthotopically engrafted OV-90^{luc+} mice (n = 16) were used as a model for the cytoreductive survival surgeries. After four weeks, once an ovarian tumour had established and disseminated to the surrounding tissues, the animals were randomised into two surgical groups; CD24 fluorescent image-guided (n = 8) or control white light surgery (n = 8). Mice assigned to FIGS (n = 8) were then injected with 3 μg/g CD24-AF750 48 h pre-operatively. The anaesthetic and analgesic protocol is described above, in addition the mice received infiltration anaesthesia of the incision line with a combination of 10 mg/kg lidocaine and 3 mg/kg bupivacaine (cat# 0839006 Bupivicaine Accord and (cat# 579092 Lidocaine Accord, Accord Healthcare AB, Solna, Sweden). The animal was placed in dorsal recumbence, the surgical area was prepared aseptically as described above, and a midline coeliotomy was performed. Abdominal exploration to assess the extent of the tumour load was performed based on visual inspection and palpation of tissues and the main tumour burden was considered resectable in all mice, lesions on vital organs (when present) were not resected. The control group underwent ovariohysterectomy and tumour resection based on this assessment. In the CD24-targeted fluorescence image-guided surgery group, the laser excitation source (λ_{ex} = 760 ± 3 nm, Supplementary Fig. S1a) was deployed after initial exploration, and tumour resection was performed with fluorescence guidance. The abdominal cavity and skin were closed in two layers with a continuous suture of 6–0 absorbable polyglactin. Postoperatively, all animals were given a subcutaneous injection of sterile saline and allowed to recover in a warm environment. The resected tumour tissue was imaged with the FLARE system for fluorescence verification, and then by BLI as described above to confirm OV-90^{luc+} origin. The post-mortem examination included macroscopic description of primary and metastatic tumours, and *ex vivo* bioluminescence and fluorescence imaging of explanted organs. Tumour lesions were submitted for histopathological analysis. FIGS image analysis was performed as described above.

2.8.6. Preclinical disease staging

We developed a modified staging system, based on the *FIGO staging classification for cancer of the ovary, fallopian tube and peritoneum* [4], and allocated a disease stage from I to IV for each mouse, based on the extent of the disease seen in pre-surgical whole-body bioluminescence images and the intraoperative assessment, where stage I indicates local disease only, stage II indicates disease within the pelvic cavity, stage III indicates disease present in elsewhere in the abdominal cavity and stage IV indicates the presence of disease

outside the abdominal cavity (Fig. 4(d)). Mice were monitored weekly by BLI and sacrificed in accordance to the study endpoints and institutional guidelines.

2.9. Immunohistochemistry

Resected tissue samples were fixed in 4% paraformaldehyde and embedded in paraffin. Formalin fixed paraffin embedded (FFPE) samples were sectioned and prepared for immunohistochemical staining of rabbit anti-human antibodies: CD24 (Cat# ab199140, Clone: polyclonal, 1:2000, Abcam, Cambridge, UK), CK8 (Cat# ab193094, Clone: EP1628Y, 1:1500, Abcam) and folate receptor alpha (Cat# PA5-24186, clone SA170417DD, 1:2000, Invitrogen). Deparaffinisation was done manually for 20 min in xylene, and hydrated through 100%, 95% and 70% ethanol to water. Antigen retrieval was done by cooking the slides for 15 min in citrate buffer (pH 6•0) in the microwave. The DAKO Envision protocol was used for the immunohistochemistry procedure. Rabbit specific polymer-HRP was used in order to avoid false-positive mouse-mouse cross bindings in the mouse tissue. Stained tissue sections were evaluated using an immunoreactivity scoring system defined by the sum of staining intensity (1 = weak, 2 = moderate, 3 = strong) and staining extent (0 = 0%, 1 = 1–5%, 2 = 6–25%, 3 = 26–75%, 4 = 76–100%) resulting in an immunoreactivity score (IRS) of 0–7 [27]. Ovarian tissue from a healthy mouse of the same breed and age was used as control, the sample was prepared as described above and stained with CD24.

2.10. Statistical analysis

Statistical analysis was performed using the GraphPad Prism software (Version 6•0, La Jolla, CA, USA). To test for significant difference between two variables, we used ordinary one-way ANOVA with two-tailed nonparametric unpaired Mann–Whitney *U* test. *P*-values $<0•05$ were regarded statistically significant. All data with error bars is presented as mean ± standard deviation.

3. Results

3.1. CD24 expression in EOC cell lines and patient-derived tumour cells

We have previously demonstrated that CD24 is a suitable target for non-invasive molecular imaging of EOC [25]. To determine the targeting capacity and intraoperative detectability of the CD24-AF750 tracer, we investigated the expression of CD24 in clinically relevant cell lines and patient-derived xenograft tumours. *In vitro* expression of CD24 in EOC cell lines OV-90, Caov-3, COV318 and Skov-3 was assessed after staining with CD24-AF750, and flow cytometric analysis revealed heterogeneous expression among cell lines (Fig. 1(a)). Quantitative determination of antigenic CD24 expression in the OV-90 cell line by flow cytometry revealed more than 300,000 CD24 binding sites per cell (Fig. 1(b)). Heterogeneous mean fluorescence intensity (MFI) results of CD24-AF750 stained cell pellets ($2•5 \times 10^6$ tumour cells) was observed in the same four HGSOC cell lines when imaging was performed with the NIR fluorescence intraoperative system, and the CD24 expression correlated with that of the flow cytometry results. Comparison of the MFI with cell pellets stained with CD24-IRDye 800CW revealed significantly lower MFI (118•1 ± 101•2 AF750 *vs*34 ± 31•4 IRDye 800CW, $p = 0.0005$), which is likely the result of suboptimal excitation of the IRDye 800CW (Fig. 1(c)). To further elucidate CD24 as a target for FIGS in the clinical setting, we performed immunohistochemistry on four different

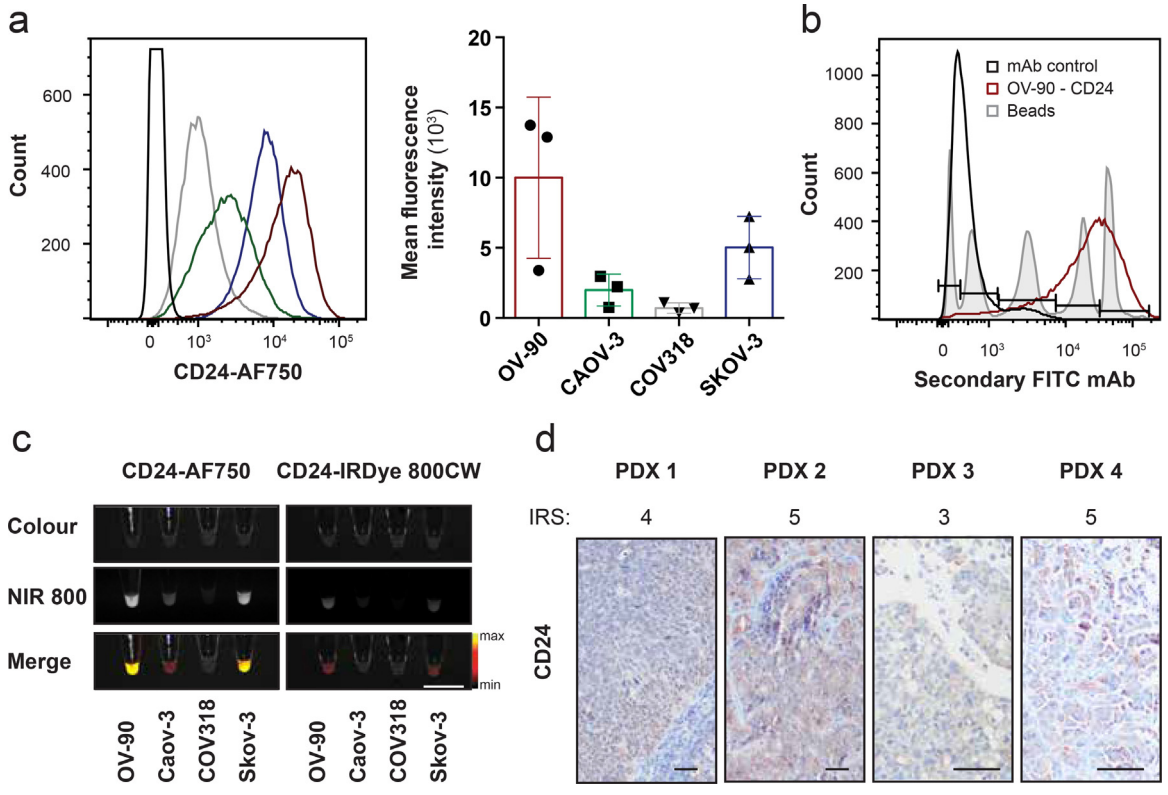

Fig. 1. CD24 is highly expressed in ovarian cancer cell lines and primary ovarian cancer cells, and can be detected by CD24-AF750 NIR staining. (a) Flow cytometry analysis of EOC cell lines OV-90, Caov-3, COV318 and Skov-3 stained with the monoclonal antibody CD24 conjugated to AF750 ($n = 3$). Each column represents the mean with SD. (b) CD24 expression was evaluated by flow cytometry, and antigen-binding capacity was quantified for OV-90 compared to monoclonal IgG1 antibody (mAb) control. (c) Validation of target-specific binding. White light (colour) image, near infrared (NIR 800) fluorescent image and pseudo-coloured fluorescence intensity merge image of CD24-AF750 stained EOC cell pellets ($2•5 \times 10^7$ tumour cells, scale bar = 1 cm). (d) Immunohistochemistry of four different patient-derived xenograft (PDX) ovarian tumours, stained with anti-CD24. Immunoreactivity score (IRS) 4•25 ± 0•96 (scale: 1ow = 1 – 7 = high). Images were captured at 100× and 200× magnification (scale bar = 25 μm).

orthotopically implanted PDX tumours, which demonstrated CD24 expression (IRS 4•25 ± 0•96; score: low = 1 – 7 = high) in patient-derived HGSOC samples (Fig. 1(d)). Finally, the safety of the CD24-AF750 conjugate was assessed *in vitro* by quantification of proliferative cells, and the assay demonstrated that increasing concentrations of CD24-AF750 have no effect on cell proliferation (Supplementary Fig. S1c).

3.2. *Determination of optimal imaging parameters* in vivo

3.2.1. *Biodistribution of CD24-AF750*

Having determined that CD24 is highly expressed in the majority of HGSOC preclinical samples analysed, we aimed to identify the optimal pharmacological parameters towards FIGS application *in vivo*. We evaluated the *in vivo* biodistribution of CD24-AF750 in an orthotopic and subcutaneous OV-90^{luc+} xenograft model by optical non-invasive FLI imaging, performed at 24-h intervals, and BLI imaging was performed to verify tumour specificity in the FLI scans (n = 3) (Fig. 2(a)). Orthotopic and subcutaneous tumours could be identified after 24 h, but the background fluorescence from the bladder, liver and kidneys were most prevalent at this time point. CD24-AF750 fluorescence in orthotopic and subcutaneous tumours reached their maximum after 48 h and 72 h, respectively, whilst the background fluorescence in the kidney and liver decreased from 24 h after administration. The tumour to background ratio (TBR) was calculated, showing a TBR of 5•47 ± 0•92 and 6•32 ± 3•44 at 48 h and 5•42 ± 1•38 and 8•16 ± 5•13 at 72 h for the orthotopic and subcutaneous tumour respectively (Fig 2(b)). Therefore, intraoperative *in vivo* imaging was performed after 48 (n = 3) and 72 (n = 3) hours, and the mean fluorescence intensity (MFI) and TBR in the primary tumour were compared, whereby an area of abdominal muscle was selected as background (Fig. 2(c)). *In vivo* the ovarian tumour MFI (102•36 ± 20•55) and TBR (2•77 ± 0•97) were higher at 48 h compared to 72 h (MFI 81•09 ± 28•75 and TBR 2•68 ± 0•99) (Fig. 2(d)).

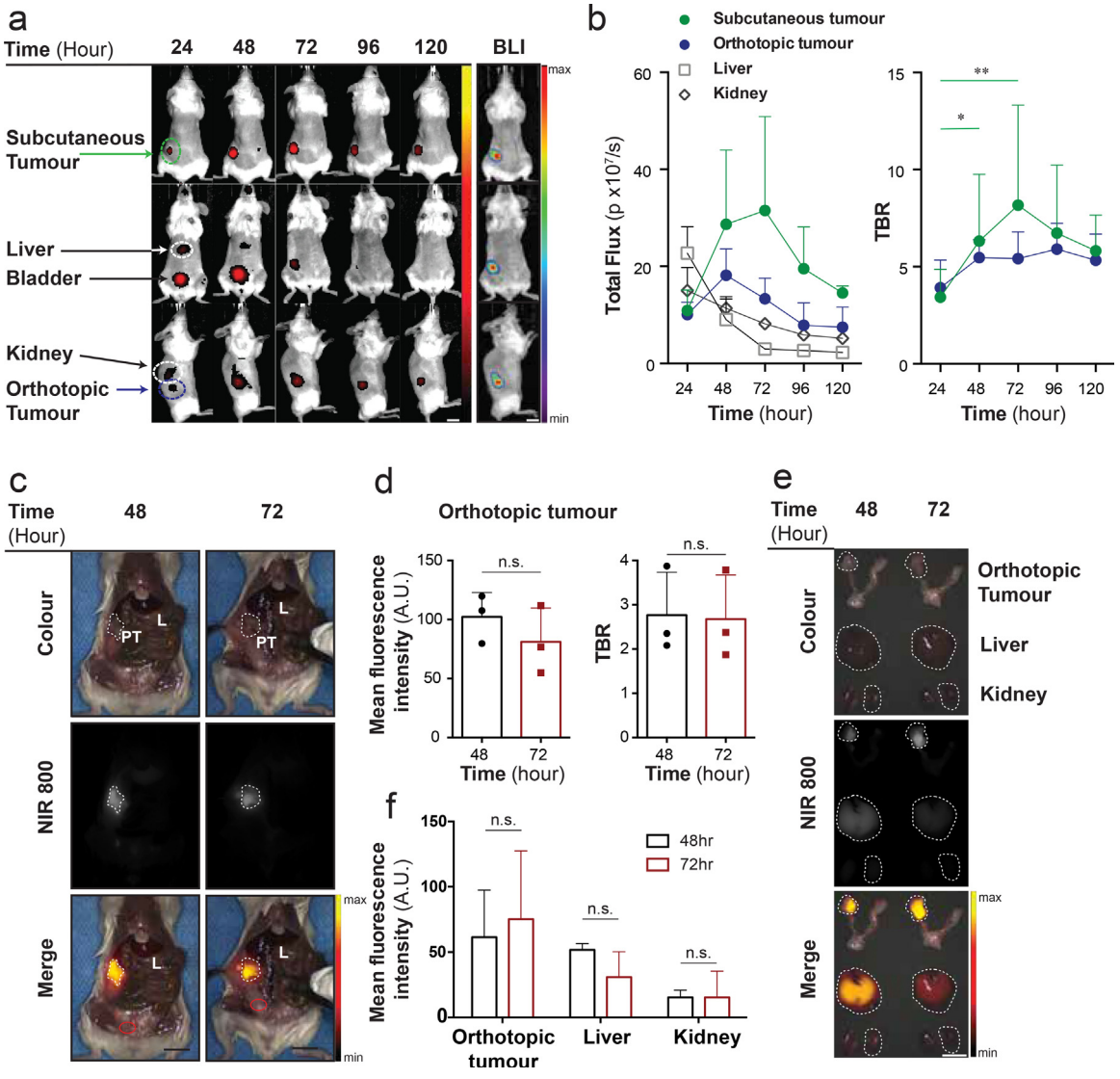

Fig. 2. Biodistribution and pharmacokinetics of CD24-AF750. (a) Representative example of longitudinal whole-body fluorescence imaging with CD24-AF750 in an OV-90 subcutaneous and orthotopic xenograft model, performed at 24-h intervals, and bioluminescence imaging (BLI) for confirmation of tumour specificity. (b) Timepoint analysis of the total fluorescence from CD24-AF750 in the subcutaneous tumour, the orthoptic tumour, liver and kidney (n = 3) identified 24 and 48 h as most advantageous. (c) Intraoperative *in vivo* images of the CD24-AF750 fluorescence in the primary tumour (marked by the dashed line) at 48 and 72 h, showing white light colour image, NIR fluorescence image and pseudo-coloured fluorescence intensity merge image. PT= primary tumour, L= liver. Tumour to background ratios (TBR) were calculated using the mean fluorescence intensity of muscle tissue as background (red circle) (d) Comparison of *in vivo* primary tumour mean fluorescence intensity (measured in arbitrary units; A.U.) and TBR. (e) Representative colour, NIR 800 and pseudo-coloured fluorescent signal merge image of the primary tumour, kidney and liver (all delineated by the dashed lines) at 48 and 72 h, used for (f) *ex vivo* MFI measurements. Statistical analysis (one-way ANOVA with unpaired Mann–Whitney U test) with $p < 0•05$ (*) were regarded as statistically significant. (Scale bars = 1 cm).

CD24 expression was confirmed by IHC in the fluorescence positive OV-90^{luc+} xenografted tumours, (IRS 4•5 ± 0•7; score: Low = 1 – 7 = high) (Supplementary Fig. S2a), and a healthy mouse ovary (NSG) was used as negative control (Supplementary Fig. S2b). *Ex vivo* measurement of the ovarian tumour MFI was 61•40 ± 36•02 at 48 h and 75•29 ± 52•25 at 72 h, whilst the liver MFI was 51•63 ± 4•90 at 48 h and 30•83 ± 19•50 at 72 h, and the kidney MFI was 15•26 ± 5•58 at 48 h and 15•28 ± 20•11 at 72 h (Fig. 2(e) and (f)). *Ex vivo* comparison of all organs is presented in Supplementary Fig. S3a. *Ex vivo* optical BLI and FLI confirmed fluorescence specificity (Supplementary Fig. S3b). The optimal time point for intraoperative imaging was identified as 48 h after CD24-AF750 injection, although tumours could be detected up to 120 h, demonstrating the long retention time of CD24-AF750 (Fig. 2(a) and (b)).

3.2.2. Determination of optimal CD24-AF750 dose

Based on our previous work [28], we identified four different doses of CD24-AF750 (1, 2, 3 and 4 μg per gram mouse bodyweight) to be compared *in vivo* for optimal intraoperative visualisation of orthotopic OV-90^{luc+} tumours (n = 3 mice per dose). When metastatic disease was detected by BLI, tumour-bearing mice were injected with CD24-AF750 and intraoperative imaging performed 48 h later (Fig. 3(a)). While tumour fluorescence showed a significant increase in MFI (45•74 ± 20•76, 94•03 ± 13•97, 100•18 ± 4•06 and 125•99 ± 65•94 respectively) with increasing antibody concentration, similar increases in background were also observed (Fig. 3(a) and (b)). The observed dose response effect may be resultant of several factors *e.g.* saturation of CD24 receptor binding sites on tumour cells, fluorescence quenching and nonspecific background binding, leading to increased background signal [29]. Thus, the TBR was calculated for each dose, using an area of abdominal muscle as background (2•31 ± 0•39, 2•77 ± 0•97, 3•28 ± 0•12 and 3•17 ± 0•23 respectively) demonstrating the highest TBR with 3 μg/g CD24-AF750 dose (p = 0.0142; Fig. 3(b)).The overall increase in liver to background ratio (2•16 ± 0•37, 1•86 ± 0•31, 2•43 ± 0•53 and 2•49 ± 0•08 respectively) with increasing dose *in vivo* resulted in a decreasing tumour to liver ratio (1•10 ± 0•28, 1•62 ± 0•54, 1•39 ± 0•29 and 1•27 ± 0•05 respectively), suggesting saturated receptors and

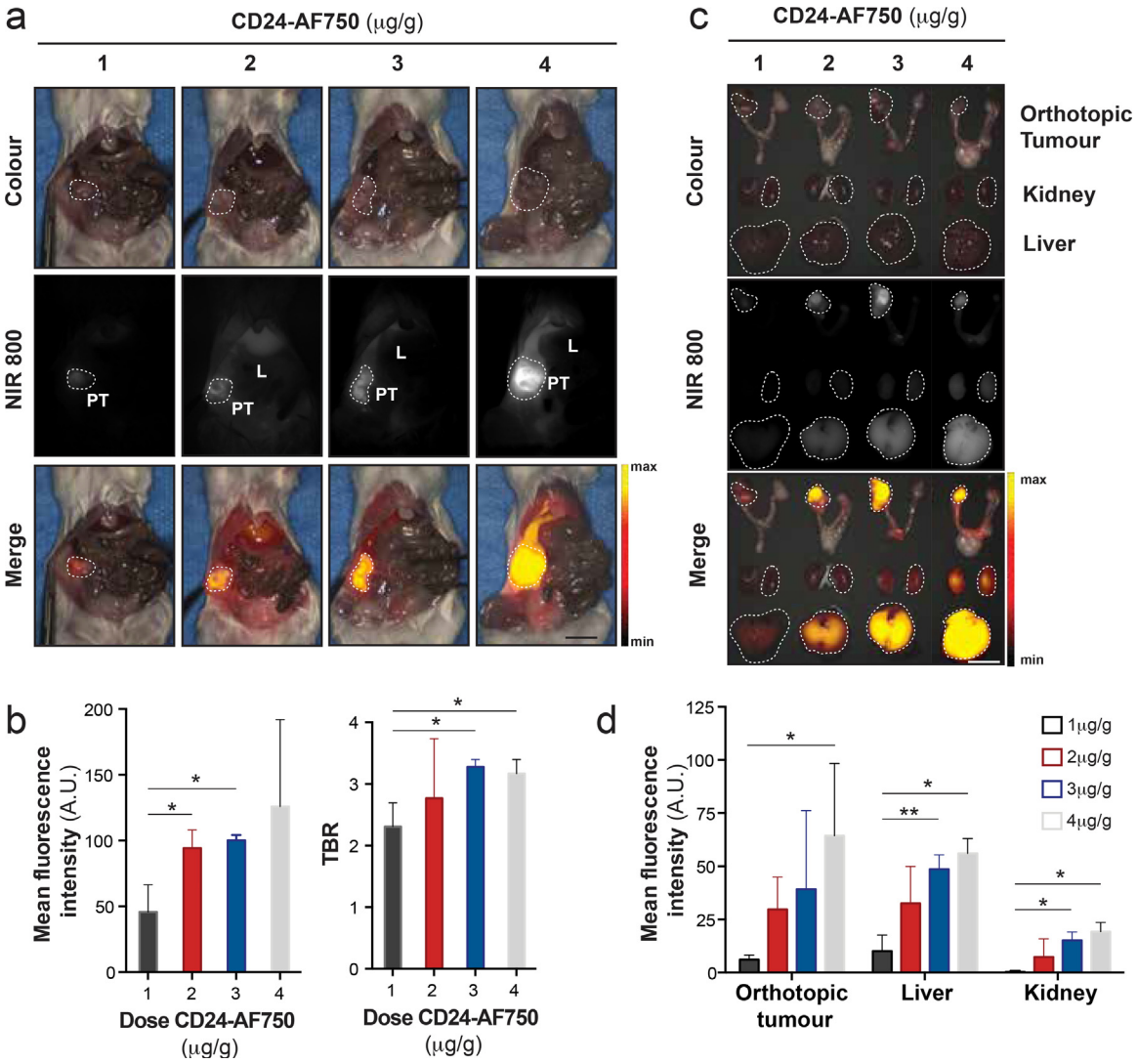

Fig. 3. Determination of the optimal dose for CD24-targeted intraoperative imaging. (a) Intraoperative *in vivo* white light (colour) image, near infrared (NIR 800) fluorescent image and pseudo-coloured fluorescence intensity merge image of representative orthotopic OV-90 xenograft models injected with 1, 2, 3 or 4 μg/g of CD24-AF750 48 h before imaging. (PT= primary tumour, marked by white dashed line, and L = liver). (b) Comparison of CD24-AF750 mean fluorescence intensity (MFI) (p = 0.0288 for 1 μg *vs* 2 μg; p = 0.0112 for 1 μg *vs* 3 μg) and tumour to background ratio (TBR) (p = 0.0142 for 1 μg *vs* 3 μg; p = 0.029 for 1 μg *vs* 4 μg) of the *in vivo* primary tumour between the four different doses. (c) *Ex vivo* colour, NIR 800 and pseudo-coloured fluorescent signal merge image of the primary tumour, kidney and liver (all marked by white dashed line) and (d) comparison of *ex vivo* MFI of the organs between the four different doses. (p = 0.0222 for 1 μg *vs* 4 μg). Statistical analysis (one-way ANOVA with unpaired Mann–Whitney U test) with $p < 0•05$ (*) were regarded as statistically significant. (Scale bars = 1 cm).

clearance (Supplementary Fig. S3c). The MFI of the primary tumour, liver and kidneys were measured *ex vivo* (Fig. 3(c)), confirming an increase with dose (primary tumour: 5•96 ± 2•24, 29•73 ± 15•21, 39•24 ± 36•93 and 64•28 ± 34•09; liver: 10•08 ± 7•44, 32•51 ± 17•41, 48•60 ± 6•79 and 56•11 ± 7•00; and kidneys 0•30 ± 0•38, 7•36 ± 8•57, 15•19 ± 3•90 and 19•23 ± 4•38) (p = 0.0222; Fig. 3(d)). *Ex vivo* optical BLI and FLI confirmed fluorescence specificity (Supplementary Fig. S3d). Based on the TBR calculated *in vivo*, 3 μg/g CD24-AF750 was employed in all further preclinical validation of CD24-AF750.

3.3. *CD24-targeted FIGS greatly enhanced metastases detection and resection* in vivo

To elucidate the potential clinical utility of CD24-guided FIGS to improve surgical guidance and increase cytoreduction, we designed a preclinical survival study comparing white light surgery with CD24-AF750 intraoperative FIGS. Orthotopic OV-90^{luc+} xenografts (n = 8 mice per group) underwent cytoreductive surgery on day 29 ± 2•4 after implantation, following determination of disease stage by BLI imaging (data not shown). Primary tumour resection and complete ovariohysterectomy was performed in all mice, and visible and resectable metastases were removed (Fig. 4(a)). BLI was performed on all the resected lesions, which confirmed fluorescence specificity from OV-90^{luc+} tumour tissue. Significantly more tumour lesions (n = 36) were identified in the CD24-FIGS cohort compared to the white light surgery group (n = 19; p = 0•0137). The total weight of resected metastatic tumour lesions was also significantly higher (72•99 ± 10.5 mg *vs*. 34•54 ± 13•62 mg, p = 0•0421) in the CD24-FIGS group (Fig. 4(b)).

Surgical resection time (Control: 9•25 ± 2•6 min; CD24-FIGS: 12•74 ± 2•2 min) was longer in the CD24-FIGS group, but did not differ significantly (p > 0•05). The postoperative-surgical mortality rate for both groups was 25% (2/8). At the first post-surgical BLI time point, seven days after surgery, the BLI signal had decreased by more than 58% (0•42 ± 0•34) in the CD24-FIGS cohort compared to 9% (0•91 ± 0•70) in the control group (p > 0•05) (Fig. 4(c)). Both groups developed an increased tumour burden at subsequent imaging time points, with a disease latency of four to six weeks, but the BLI signal of the CD24-FIGS cohort was consistently lower than that of the control group (Fig. 4(c)). To evaluate if disease stage at the time of surgery impacted the post-surgical outcome in the ovarian xenograft models, we developed a preclinical staging system, modified from the *FIGO staging classification* (Fig. 4(d)), as described earlier. The majority of the mice were in stage II and III at the time debulking surgery was performed. In mice with stage I disease, the post-surgical BLI values were almost zero, indicating close to complete cytoreduction in both groups (Fig. 4(e), Supplementary Fig. S4). CD24-FIGS had the highest impact during debulking surgery in stage II of our model (Fig. 4(f), Supplementary Fig. S4). Mice allocated to stage III had tumour lesions that were unresectable at the time of debulking surgery, and therefore the decrease in the average bioluminescence intensity was only minor in both cohorts (Fig. 4(g), Supplementary Fig. S5).

3.4. *Verification of CD24-AF750 targeting ability in heterogeneous patient-derived xenograft models*

CD24-guided FIGS greatly improved the detection of metastases in our orthotopic xenograft model of HGSOC. To further verify the translational potential of CD24-AF750 for intraoperative guidance during debulking surgery in ovarian cancer, we imaged four different, clinically annotated orthotopic PDX models of metastatic HGSOC with heterogeneous CD24 expression (n = 10). After injection with 3 μg/g CD24-AF750 48 h prior to intraoperative fluorescence imaging, CD24-AF750 specifically identified the primary tumour and small metastatic tumour lesions in the omental tissues, liver, intestines and diaphragm in the various PDX models, and *ex vivo* FLI confirmed fluorescence signal specificity (Fig. 5(a)). CD24 expression in PDX fluorescence positive lesions was confirmed by IHC, with IRS ranging from 4 to 6 (4•4 ± 1•1, score; low = 1−7 = high), demonstrating heterogeneous expression in PDX tumour lesions. CK8 staining confirmed human tumour origin (Fig. 5(b)). IHC staining against folate receptor alpha was performed to compare the expression to that of CD24 in the patient-derived tumours, demonstrating comparable IRS (p > 0•05, n = 21) (Fig. 5(c)). Intraoperative CD24-guided FIGS in orthotopic PDX models of metastatic HGSOC, representing patient tumour heterogeneity and dissemination, allow for specific identification of primary tumours and small metastatic lesions.

4. Discussion

Physiological CD24 expression is restricted to pre-B-cells, neutrophils and stem cells in healthy tissues and has been correlated with higher self-renewal ability, chemotherapy resistance, omental, peritoneal and lymph node metastasis and decreased survival in HGSOC [24,30,31]. Coupled with an abnormal upregulation of CD24 in multiple human carcinoma (68% and more specifically, 91% in ovarian carcinomas), has prompted its exploitation as a therapeutic biomarker [32−34]. Consequently, several reports have described therapeutic approaches including CAR [35], antibody conjugates [36,37], and bispecific antibodies [38] targeting CD24. Here we demonstrate the suitability of a CD24 antibody conjugate (CD24-AF750) for intraoperative FIGS in clinically relevant models of HGSOC, supporting its potential for translation in the intraoperative setting for ovarian cancer patients. Apart from methylene blue and indocyanine green, which have relatively low quantum yields and strong non-specific binding [39] no NIR fluorescent contrast agents have received clinical approval yet. Although the NIR fluorophore IRDye 800CW conjugated to clinically approved theragnostic monoclonal antibodies is currently in clinical trials [13,14] there is no evidence of the superiority of any NIR contrast agent yet. We chose Alexa Fluor 750 based on the spectral properties (quantum yield, molar extinction coefficient and Stokes shift), along with its compatibility with the spectral sensitivity of our image guided surgery system.

One of the major challenges in application of murine models to the FIGS setting is in the clinical relevance of the model. Typically, researchers have applied subcutaneous xenograft models to validate targeted imaging approaches, however, these models have little to no clinical relevance in disseminated cancers [20,21,23]. Ceppi et al. addressed this limitation by utilising an intraperitoneal ovarian cancer xenograft model to demonstrate the survival advantage of targeting SPARC in the FIGS setting [22]. We have previously developed a surgically relevant orthotopic model of HGSOC [26,40]. In the current study we build upon this by employing OV-90^{luc+} and PDX orthotopic xenograft models, where disease dissemination better mimics clinical characteristics of HGSOC [25]. To increase the clinical translatability of our work we introduce a preclinical staging system based on FIGO staging used clinically in EOC patients (Fig. 4(d)) and utilise pre-surgery whole-body BLI for surgical planning.

FIGS employing CD24-AF750 permitted detection of significantly more metastases (47•3%) compared to guidance by white light and palpation alone in OV-90^{luc+} orthotopic xenograft models. At the optimal dose of 3 ug/ug, CD24-AF750 FIGS could also identify primary and metastatic lesions in orthotopic PDX models with heterogeneous CD24 expression. Orthotopic PDX models can provide a good indication of how well the tracer will perform in a heterogenous human cancer patient population, however, one limitation to this model is that non-specific uptake of the tracer cannot be accurately assessed when the target is human specific [14]. Pre-surgical BLI was found to correlate well with observed intraoperative disease dissemination, and mice in our preclinical stage I and II (Fig. 4(d)) could have

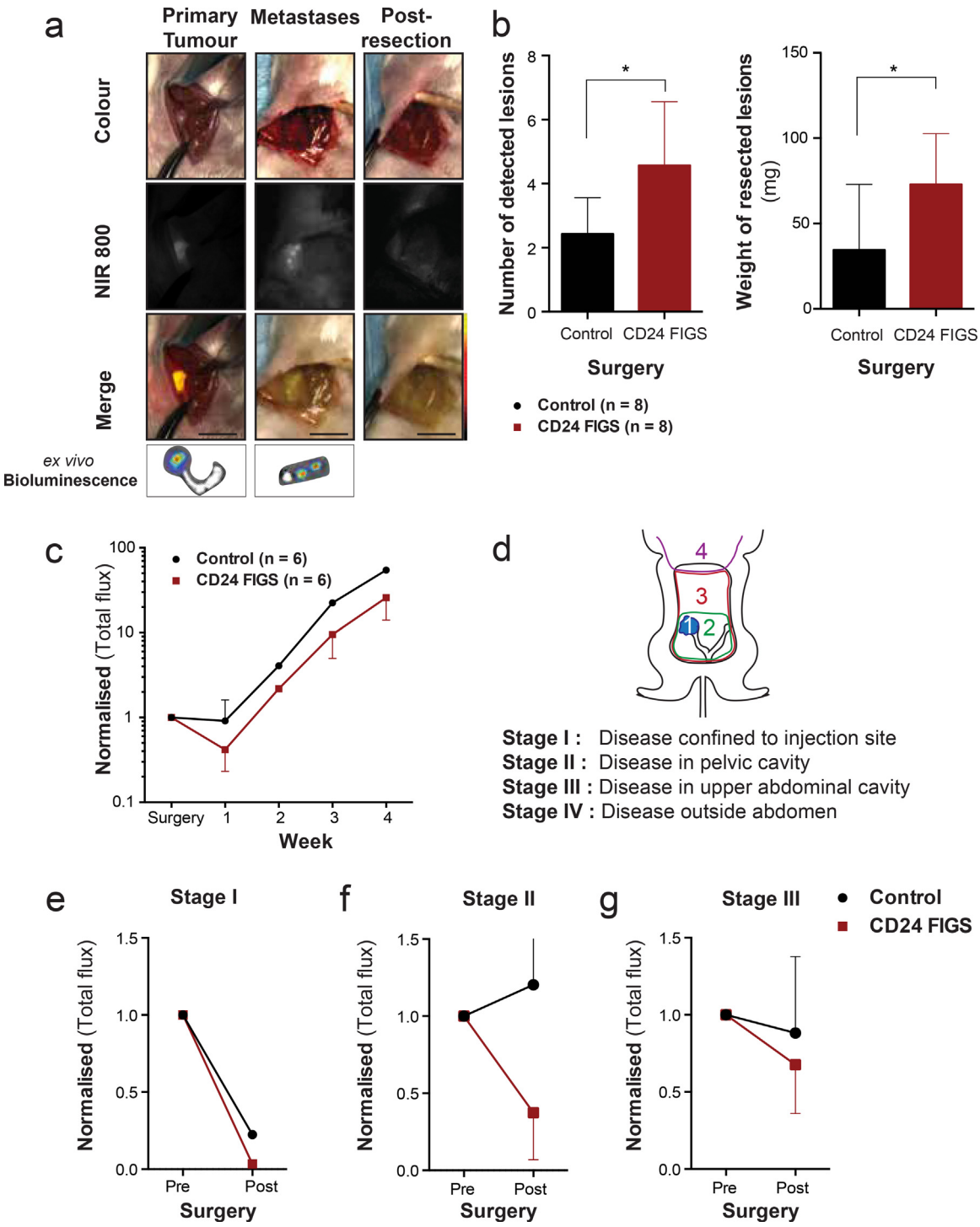

Fig. 4. Survival surgery in OV-90^{luc+} orthoptic xenografts. (a) Intraoperative white light (colour), near infrared (NIR 800) fluorescent and pseudo-coloured fluorescence intensity merge images from CD24-targeted fluorescence image-guided surgery (FIGS) of the primary ovarian tumour and intra-abdominal metastases. *Ex vivo* bioluminescence imaging was performed on resected lesions to confirm tumour specificity. (Scale bars = 1 cm). (b) Comparison of the number and total weight of resected metastatic lesions between the CD24 FIGS cohort (n = 8) and white light control surgery (n = 8). (c) Comparison of post-operative bioluminescence signal intensity between CD24-FIGS resected mice (n = 6) and white light control mice (n = 6). Longitudinal whole-body bioluminescence imaging was performed weekly for four weeks post-surgery and the bioluminescent signal was normalised to the presurgical bioluminescence signal of each individual mouse. (d) Mice were allocated a disease stage based on pre-surgical bioluminescence signal and intraoperative disease dissemination (e) Comparison of (normalised) pre- and post-surgical bioluminescence signal between CD24-FIGS and white light surgery in Stage I (f) Stage II and (g) Stage III resected mice ($p > 0{\bullet}05$). Statistical analysis (Mann–Whitney U test) with $p < 0{\bullet}05$ (*) were regarded as statistically significant.

satisfactory tumour resections, highlighting the utility of a CD24 targeted approach for FIGS in HGSOC. However, the small size of rodents makes debulking surgery technically challenging, and certain procedures, for instance intestinal resection with end-to-end anastomosis, impossible. Subsequently, mice with metastases on vital organs could not undergo resection resulting in similar debulkment results between CD24-FIGS and controls at stage III (Fig. 4(g), Supplementary Fig. S4). These results, however, are not reflective of the efficacy of CD24-AF750 tumour delineation, but rather highlight the disadvantage of mouse models for surgical applications. Thus, future

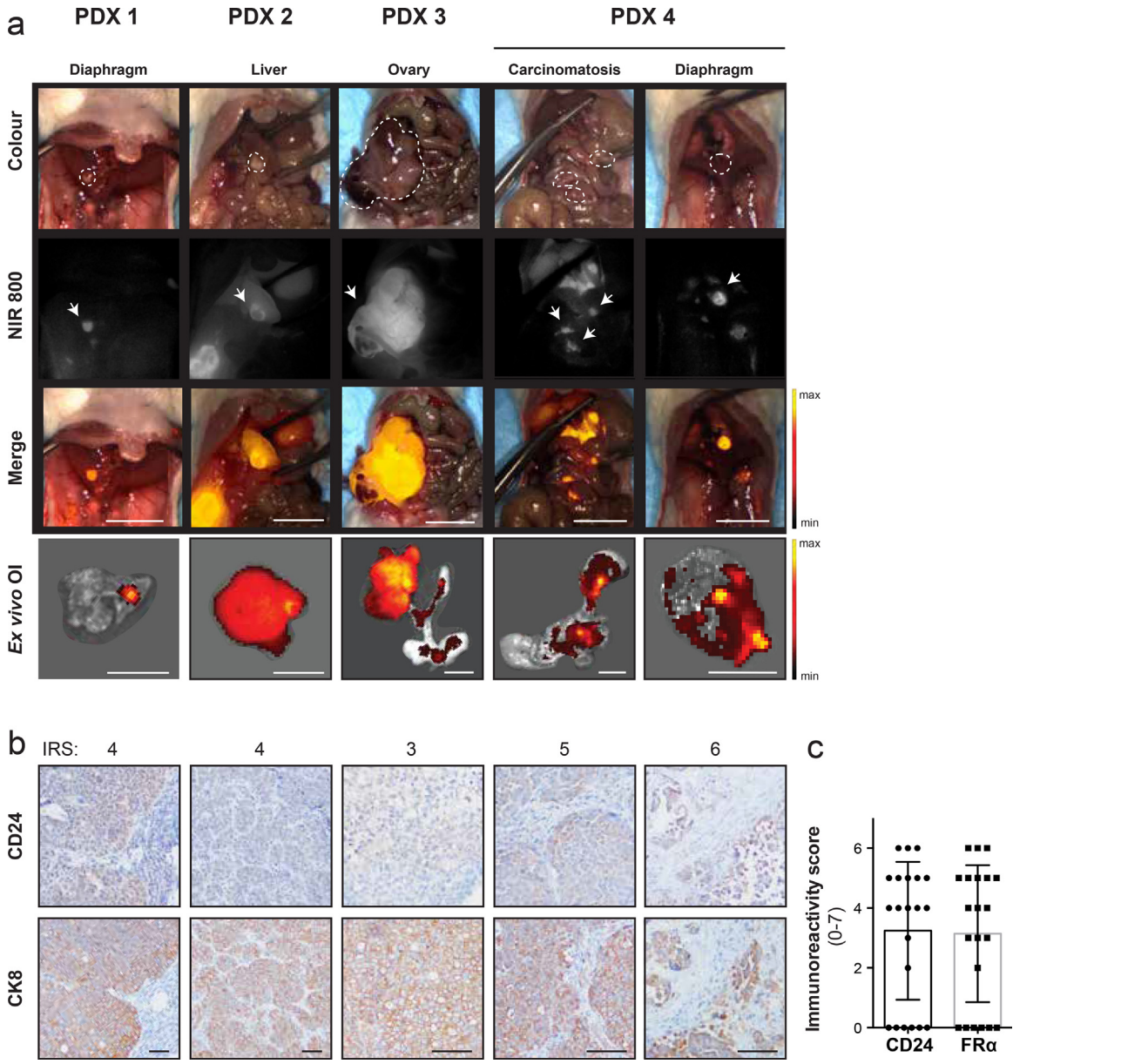

Fig. 5. Intraoperative CD24-targeted fluorescence imaging of four heterogeneous PDX of advanced stage HGSOC. (a) Intraoperative white light (colour), near infrared (NIR 800) fluorescent and pseudo-coloured fluorescence intensity merge images show positive identification of primary tumour and small metastatic lesions in four separate, orthotopically implanted PDX models of HGSOC, after injection with 3 μg/g CD24-AF750 48 h prior to intraoperative fluorescence imaging. *Ex vivo* optical imaging confirmed fluorescence specificity. Positive lesions are represented by dashed lines in the colour view image. The arrow points to the strongest fluorescent signal in the near infrared (NIR) 800 images. (Scale bar, 1 cm). (b) CD24 expression was confirmed by IHC in fluorescence positive PDX lesions. CD24 staining was evaluated in all five resected lesions with an immunoreactivity score (4•4 ± 1•1, scale: low 1 – 7 high). CK8 staining was used to confirm human tumour origin. Magnification 200×. (c) CD24 and folate receptor alpha IHC immunoreactivity score comparison on PDX tissue sections, demonstrating no significance ($p > 0$•05, Mann–Whitney *U* test)) difference ($n = 21$). Images were captured at 100× and 200× magnification (scale bar = 25 μm).

preclinical development of FIGS probes should also consider companion animal models as an ethically attractive large animal alternative [41]. Veterinary clinical trials in pet dogs with naturally occurring cancer can accelerate the definition of safety profiles and biological activity of new tumour targeted fluorescent probes and fill the gap between the laboratory animal models and early-phase clinical studies in patients [42].

As demonstrated by van Dam et al. in 2011, intraoperative tumour-targeted fluorescence image-guided surgery has the potential to improve the degree of cytoreduction and improve survival in patients with advanced ovarian cancer [16,18,19]. While FR demonstrates high expression in EOC, it is not expressed ubiquitously in all EOC patients. Indeed, a study of tumour samples from 2801 patients in the Ovarian Tumour Tissue Analysis (OTTA) consortium found FR expression ranged from 76% in HGSOC to 11% in mucinous carcinomas [43]. While no such studies have investigated CD24 expression in such a large patient cohort, this data highlights the need for additional targets for FIGS applications in clinically heterogeneous cohorts. Furthermore, FR expression is associated with increased overall survival [43], with no major changes in receptor expression in matched pre- and post-treatment biopsy samples [44]. In contrast, CD24 is a known cancer stem cell marker [24], promotes motility and metastasis [45] and is a predictor of tumour recurrence [46]. Thus, a CD24 targeted FIGS probe could be multiplexed with a FRα contrast reagent to increase tumour delineation in primary cytoreductive surgery. Finally, CD24 FIGS probe could be an excellent candidate for secondary debulkment protocols [47].

We have demonstrated that CD24-targeted fluorescence image-guided surgery significantly improved cytoreduction in clinically relevant orthotopic models of high-grade serous ovarian carcinoma, and we have demonstrated the ability of CD24-AF750 to identify metastatic lesions in various heterogenous patient-derived xenograft models. The addition of CD24 as a promising biomarker for the application of fluorescence-guided surgery can aid further delineation of metastases and be of greater benefit to ovarian cancer patients with poor prognosis.

Declaration of Competing Interest

The authors declare that they have no conflicts of interest.

Acknowledgement

The authors acknowledge the support from the MARIE SKLODOSWKA-CURIE ACTION (proposal number 675743; acronym ISPIC) carried out within the H2020 program MSCA-ITN funded by the EU. The authors would like to thank Mark Bordo from Curadel LCC for technical support and help with the intraoperative imaging system. The authors acknowledge the Flow Cytometry Core Facility and the Molecular Imaging center, Department of Clinical Science, University of Bergen.

Funding sources

Katrin Kleinmanns and Vibeke Fosse are part of the project "Image-Guided surgery and Personalised Postoperative Immunotherapy to Improving Cancer Outcome" (ISPIC) funded though the H2020 program MSCA-ITN under grant agreement number 675743. Ben Davidson received financial support from Inger and John Fredriksen Foundation for Ovarian Cancer Research. Elvira García de Jalón received financial support from the University of Bergen (815900). Olav Tenstad received funding through Regional Health Authorities (Helse-Vest; 911974). Financial support from Helse Vest RHF and Helse Bergen HF (project numbers 911809, 911852, 912171, 240222, HV1269) as well as The Norwegian Cancer Society (182735) and The Research Council of Norway through its Centers of excellence funding scheme (project number 223250, 262652) has been granted to Line Bjørge and Emmet McCormack. The Funding sources had no involvement in the writing, collection, analysis, interpretation or submission of the study and full access to the study data was provided.

Supplementary materials

Supplementary material associated with this article can be found in the online version at doi:10.1016/j.ebiom.2020.102783.

References

[1] Lheureux S, Braunstein M, Oza AM. Epithelial ovarian cancer: evolution of management in the era of precision medicine. CA Cancer J Clin 2019;393(10177):1240–53.
[2] Bowtell DD, Bohm S, Ahmed AA, et al. Rethinking ovarian cancer II: reducing mortality from high-grade serous ovarian cancer. Nat Rev Cancer 2015;15(11):668–79.
[3] du Bois A, Reuss A, Pujade-Lauraine E, Harter P, Ray-Coquard I, Pfisterer J. Role of surgical outcome as prognostic factor in advanced epithelial ovarian cancer: a combined exploratory analysis of 3 prospectively randomized phase 3 multicenter trials: by the Arbeitsgemeinschaft Gynaekologische Onkologie Studiengruppe Ovarialkarzinom (AGO-OVAR) and the Groupe d'Investigateurs Nationaux Pour les Etudes des Cancers de l'Ovaire (GINECO). Cancer 2009;115(6):1234–44.
[4] Berek JS, Kehoe ST, Kumar L, Friedlander M. Cancer of the ovary, fallopian tube, and peritoneum. Int J Gynecol Obstet 2018;143:59–78.
[5] Torres D, Wang C, Kumar A, et al. Factors that influence survival in high-grade serous ovarian cancer: a complex relationship between molecular subtype, disease dissemination, and operability. Gynecol Oncol 2018;150(2):227–32.
[6] Gharpure KM, Pradeep S, Sans M, et al. FABP4 as a key determinant of metastatic potential of ovarian cancer. Nat Commun 2018;9(1):2923.
[7] Mahner S, Heitz F, Burges A, et al. TRUST: trial of radical upfront surgical therapy in advanced ovarian cancer (ENGOT ov33/AGO–OVAR OP7). Am Soc Clin Oncol 2017;35(15):TPS5602-TPS5602. doi: 10.1200/JCO.2017.35.15_suppl.TPS5602.
[8] Ghisoni E, Imbimbo M, Zimmermann S, Valabrega G. Ovarian cancer immunotherapy: turning up the heat. Int J Mol Sci 2019;20(12):2927.
[9] Riester M, Wei W, Waldron L, et al. Risk prediction for late-stage ovarian cancer by meta-analysis of 1525 patient samples. J Natl Cancer Inst 2014;106(5):dju048.
[10] Kyriazi S, Kaye SB. Imaging ovarian cancer and peritoneal metastases—current and emerging techniques. Nat Rev Clin Oncol 2010;7(7):381.
[11] Vahrmeijer AL, Hutteman M, Van Der Vorst JR, Van De Velde CJ, Frangioni JV. Image-guided cancer surgery using near-infrared fluorescence. Nat Rev Clin Oncol 2013;10(9):507.
[12] Tipirneni KE, Warram JM, Moore LS, et al. Oncologic procedures amenable to fluorescence-guided surgery. Ann Surg 2017;266(1):36–47.
[13] Hernot S, van Manen L, Debie P, Mieog JSD, Vahrmeijer AL. Latest developments in molecular tracers for fluorescence image-guided cancer surgery. Lancet Oncol 2019;20(7):e354–e67.
[14] Debie P, Hernot S. Emerging fluorescent molecular tracers to guide intra-operative surgical decision-making. Front Pharmacol 2019;10:510.
[15] Weissleder R, Ntziachristos V. Shedding light onto live molecular targets. Nat Med 2003;9(1):123.
[16] van Dam GM, Themelis G, Crane LM, et al. Intraoperative tumor-specific fluorescence imaging in ovarian cancer by folate receptor-alpha targeting: first in-human results. Nat Med 2011;17(10):1315–9.
[17] Tummers QR, Hoogstins CE, Gaarenstroom KN, et al. Intraoperative imaging of folate receptor alpha positive ovarian and breast cancer using the tumor specific agent EC17. Oncotarget 2016;7(22):32144–55.
[18] Hoogstins CE, Tummers QR, Gaarenstroom KN, et al. A novel tumor-specific agent for intraoperative near-infrared fluorescence imaging: a translational study in healthy volunteers and patients with ovarian cancer. Clin Cancer Res 2016;22(12):2929–38.
[19] Randall LM, Wenham RM, Low PS, Dowdy SC, Tanyi JL. A phase II, multicenter, open-label trial of OTL38 injection for the intra-operative imaging of folate receptor-alpha positive ovarian cancer. Gynecol Oncol 2019 S0090-8258(19):31396-4.
[20] Debie P, Van Quathem J, Hansen I, et al. Effect of dye and conjugation chemistry on the biodistribution profile of near-infrared-labeled nanobodies as tracers for image-guided surgery. Mol Pharm 2017;14(4):1145–53.
[21] Wang P, Fan Y, Lu L, et al. NIR-II nanoprobes in-vivo assembly to improve image-guided surgery for metastatic ovarian cancer. Nat Commun 2018;9(1):2898.
[22] Ceppi L, Bardhan NM, Na Y, et al. Real-time single-walled carbon nanotube-based fluorescence imaging improves survival after debulking surgery in an ovarian cancer model. ACS Nano 2019;13(5):5356–65.
[23] van Scheltinga AGT, van Dam GM, Nagengast WB, et al. Intraoperative near-infrared fluorescence tumor imaging with vascular endothelial growth factor and human epidermal growth factor receptor 2 targeting antibodies. J Nucl Med 2011;52(11):1778–85.
[24] Gao MQ, Choi YP, Kang S, Youn JH, Cho NH. CD24+ cells from hierarchically organized ovarian cancer are enriched in cancer stem cells. Oncogene 2010;29(18):2672–80.
[25] Kleinmanns K, Bischof K, Anandan S, et al. CD24-targeted fluorescence imaging in patient-derived xenograft models of high-grade serous ovarian carcinoma. EBioMedicine 2020;56:102782.
[26] Helland O, Popa M, Vintermyr OK, et al. First in-mouse development and application of a surgically relevant xenograft model of ovarian carcinoma. PLoS One 2014;9(3):e89527.
[27] Meyerholz DK, Beck AP. Principles and approaches for reproducible scoring of tissue stains in research. Lab Investig 2018;98(7):844.
[28] McCormack E, Mujić M, Osdal T, Bruserud Ø, Gjertsen BT. Multiplexed mAbs: a new strategy in preclinical time-domain imaging of acute myeloid leukemia. Blood 2013;121(7):e34–42.
[29] Koller M, Qiu S-Q, Linssen MD, et al. Implementation and benchmarking of a novel analytical framework to clinically evaluate tumor-specific fluorescent tracers. Nat Commun 2018;9(1):1–11.
[30] Nakamura K, Terai Y, Tanabe A, et al. CD24 expression is a marker for predicting clinical outcome and regulates the epithelial-mesenchymal transition in ovarian cancer via both the Akt and ERK pathways. Oncol Rep 2017;37(6):3189–200.
[31] Kristiansen G, Denkert C, Schlüns K, Dahl E, Pilarsky C, Hauptmann S. CD24 is expressed in ovarian cancer and is a new independent prognostic marker of patient survival. Am J Pathol 2002;161(4):1215–21.
[32] Davidson B. CD24 is highly useful in differentiating high-grade serous carcinoma from benign and malignant mesothelial cells. Hum Pathol 2016;58:123–7.
[33] Lee J-H, Kim S-H, Lee E-S, Kim Y-S. CD24 overexpression in cancer development and progression: a meta-analysis. Oncol Rep 2009;22(5):1149–56.
[34] Tarhriz V, Bandehpour M, Dastmalchi S, Ouladsahebmadarek E, Zarredar H, Eyvazi S. Overview of CD24 as a new molecular marker in ovarian cancer. J Cell Physiol 2019;234(3):2134–42.
[35] Klapdor R, Wang S, Morgan M, et al. Characterization of a novel third-generation anti-CD24-CAR against ovarian cancer. Int J Mol Sci 2019;20(3):660. doi: 10.3390/ijms20030660.
[36] Barkal AA, Brewer RE, Markovic M, et al. CD24 signalling through macrophage Siglec-10 is a target for cancer immunotherapy. Nature 2019;572(7769):392–6.
[37] Sun F, Wang Y, Luo X, et al. Anti-CD24 antibody-nitric oxide conjugate (ANC) selectively and potently suppresses hepatic carcinoma. Cancer Res 2019 canres.2839.018.

[38] Han Y, Sun F, Zhang X, et al. CD24 targeting bi-specific antibody that simultaneously stimulates NKG2D enhances the efficacy of cancer immunotherapy. J Cancer Res Clin Oncol 2019;145(5):1179–90.
[39] Hong G, Antaris AL, Dai H. Near-infrared fluorophores for biomedical imaging. Nat Biomed Eng 2017;1(1):1–22.
[40] Helland O, Popa M, Bischof K, Gjertsen BT, McCormack E, Bjorge L. The HDACi panobinostat shows growth inhibition both in vitro and in a bioluminescent orthotopic surgical xenograft model of ovarian cancer. PLoS One 2016;11(6):e0158208.
[41] Keating JJ, Runge JJ, Singhal S, et al. Intraoperative near-infrared fluorescence imaging targeting folate receptors identifies lung cancer in a large-animal model. Cancer 2017;123(6):1051–60.
[42] Lwin TM, Hoffman RM, Bouvet M. Advantages of patient-derived orthotopic mouse models and genetic reporters for developing fluorescence-guided surgery. J Surg Oncol 2018;118(2):253–64.
[43] Köbel M, Madore J, Ramus S, et al. Evidence for a time-dependent association between FOLR1 expression and survival from ovarian carcinoma: implications for clinical testing. An ovarian tumour tissue analysis consortium study. Br J Cancer 2014;111(12):2297.
[44] Martin LP, Konner JA, Moore KN, et al. Characterization of folate receptor alpha (FRα) expression in archival tumor and biopsy samples from relapsed epithelial ovarian cancer patients: a phase I expansion study of the FRα-targeting antibody-drug conjugate mirvetuximab soravtansine. Gynecol Oncol 2017;147(2):402–7.
[45] Baumann P, Cremers N, Kroese F, et al. CD24 expression causes the acquisition of multiple cellular properties associated with tumor growth and metastasis. Cancer Res 2005;65(23):10783–93.
[46] Liu C, Zheng S, Shen H, et al. Clinical significance of CD24 as a predictor of bladder cancer recurrence. Oncol Lett 2013;6(1):96–100.
[47] Harter P, Hilpert F, Mahner S, et al. Prognostic factors for complete debulking in first-and second-line ovarian cancer. Int J Gynecol Cancer 2009;19(Suppl 2):S14–S7.